Integrated lithium niobate Vernier micro-ring filter with wide and fast tuning capabilities

WANG, Zhenzheng; CHEN, Zhaoxi; FENG, Hanke; ZHANG, Ke; WANG, Cheng

Published in:
Optics Express

Published: 02/12/2024

Document Version:
Final Published version, also known as Publisher's PDF, Publisher's Final version or Version of Record

Published version (DOI):
10.1364/OE.535076

Publication details:
WANG, Z., CHEN, Z., FENG, H., ZHANG, K., & WANG, C. (2024). Integrated lithium niobate Vernier micro-ring filter with wide and fast tuning capabilities. *Optics Express*, *32*(25), 44272-44279. https://doi.org/10.1364/OE.535076

Research Article | Vol. 32, No. 25 / 2 Dec 2024 / Optics Express 44272
Optics EXPRESS

Integrated lithium niobate Vernier micro-ring filter with wide and fast tuning capabilities

ZHENZHENG WANG, ZHAOXI CHEN, HANKE FENG, KE ZHANG, AND CHENG WANG*

Department of Electrical Engineering & State Key Laboratory of Terahertz and Millimeter Waves, City University of Hong Kong, Kowloon, Hong Kong SAR, China
cwang257@cityu.edu.hk

Abstract: Tunable optical micro-ring filters play significant roles in optical communications, microwave photonics, and photonic neural networks. Typical micro-ring filters are based on either a thermo-optic (TO) effect with microsecond timescales or an electro-optic (EO) effect with a limited tuning range. Here, we report a continuously tunable lithium niobate on insulator (LNOI) Vernier cascaded micro-ring filter with wire-bonded packaging integrated with both TO and EO tuning electrodes, featuring a 40-nm free spectral range (FSR), 2.3 GHz EO bandwidth, and a high sidelobe suppression ratio of 21.7 dB, simultaneously. Our high-performance optical micro-ring filter could become an important element in future LNOI photonic circuits with applications in high-capacity wavelength-division multiplexing (WDM) systems, broadband microwave photonics, fast-tunable external-cavity lasers, and high-speed photonic neural networks.

1. Introduction

Optical micro-ring filters can selectively transmit, reflect, or absorb light of specific wavelengths over a wide spectral range and are critical components in many emerging applications such as wavelength division multiplexing (WDM) systems [1–4], microwave photonics [5–9], tunable external-cavity lasers [10,11], and photonic neural networks [12]. Most of these applications ideally require optical micro-ring filters that have a large free spectral range (FSR), high tuning speed, high sidelobe suppression ratio (SLSR), and low insertion loss.

To obtain a large FSR, a common method is to reduce the radius of the ring: a micro-ring resonator (MRR) with a 1.5 μm radius on a silicon on insulator (SOI) platform could support a measured FSR of 62.5 nm with a moderate intrinsic quality (Q) factor of 18,000 [13]. The trade-off between FSR and Q factor is mainly due to deteriorated radiation loss for small ring radii, and is particularly prominent for partially etched structures on lower-index platforms.

An effective approach to break this trade-off is to use the Vernier effect of double rings, which takes advantage of small differences in the radii of the two rings to increase the overall FSR [14–19]. Additionally, the Vernier effect also enables greatly improved wavelength tuning efficiency, leading to reduced power consumption compared with a single ring. However, most prior Vernier ring resonators on silicon [20,21] and silicon nitride [22] platforms perform tuning based on the thermo-optic (TO) effect, with response times generally at μs level. The recently emerged lithium niobate on insulator (LNOI) platform offers the opportunity to achieve a wide tuning range and fast tuning speed simultaneously, as it features not only TO characteristics [23,24] but also a strong electro-optic (EO) response (r_{33} = 30 pm/V) that can reach ns-level tuning [25–32]. In addition, lithium niobate is a naturally low-loss material [33], enabling designs of Vernier rings with a high SLSR and relatively high transmission at the same time. To date, however, the reported LNOI microring filters have not been able to make full use of the two effects in a single device. Achieving high-speed and wide-range tunable filters in the LNOI platform could provide significant device functionality for future high-performance integrated

#535076 https://doi.org/10.1364/OE.535076
Journal © 2024 Received 8 Jul 2024; revised 6 Sep 2024; accepted 5 Oct 2024; published 20 Nov 2024

Optics EXPRESS

LNOI photonics such as high-capacity wavelength-division multiplexing systems and broadband microwave photonics based on the LNOI platform.

Here, we fulfill such promises and demonstrate an integrated LNOI tunable Vernier cascaded micro-ring filter with both TO and EO tuning capabilities. This design allows us to achieve a large FSR of approximately 40 nm, a high EO bandwidth of 2.3 GHz, a high SLSR of 21.7 dB, and a relatively low on-resonance insertion loss of 2.5 dB, simultaneously. In addition, we interface the optical filter chip with a control printed circuit board (PCB) via wire bonding, realizing effective 4-channel electrical control of both TO and EO electrodes simultaneously.

2. Device design and fabrication

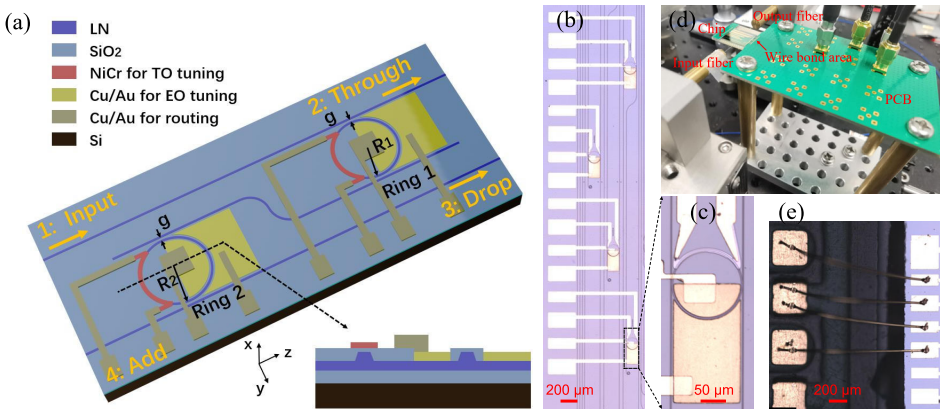

Fig. 1. (a) Schematic diagram of the double-ring filter. The cross section of the filter along the dashed line is displayed in the bottom right inset. (b-c) Microscope images of the fabricated tunable Vernier micro-ring filter with electrodes and wire bonding pads. (d) The electrically packaged optical filter module under testing. (e) Close-up microscope image of the wire bonding area.

Figure 1(a) presents the schematic diagram of the tunable Vernier cascaded micro-ring filter based on an x-cut LNOI platform, which includes two add-drop rings: ring 1 and ring 2. The left and right sides of both rings are equipped with nichrome (NiCr) TO and Cu/Au EO phase shifters, respectively. The TO phase shifters are fabricated on top of a 1.5-μm-thick cladding SiO_2 layer and positioned directly above the rings with widths of 2 μm, while the EO tuners with electrode gaps of 6 μm are placed on the two sides of the ring waveguide, as shown in the cross-section schematic in the inset of Fig. 1(a). The radius of ring 2 ($R_2 = 76$ μm) is slightly larger than that of ring 1 ($R_1 = 72$ μm), leading to a 5% smaller FSR for ring 2 (FSR_2) than that of ring 1 (FSR_1).

The devices are fabricated on a commercially available 4-inch x-cut LNOI platform with a 500-nm-thick thin film lithium niobate layer, and a 4.7-μm buried SiO_2 layer. First, plasma-enhanced chemical vapor deposition (PECVD) is used to deposit a layer of SiO_2 on the LNOI wafer. The optical filter structures are then patterned using an ASML UV Stepper lithography system die by die (1.5 cm × 1.5 cm) with a resolution of 500 nm. The patterns of the photoresist are first transferred to SiO_2 and then to the LN layer using a reactive ion etching (RIE) system with fluorine-based and Ar^+ based plasmas, respectively, resulting in a 250 nm rib waveguide and a 250 nm LN slab. Next, a 1.5 μm layer of SiO_2 is deposited to protect the LN waveguide and form optical isolation from the TO electrodes. Following this, the EO electrodes are formed through a second stepper lithography process followed by dry etching of the SiO_2 in the EO electrode area, thermal evaporation of a 1-μm-thick Cu/Au layer, and lift-off. Subsequently, the TO phase shifter (200 nm thick NiCr) is deposited through photolithography, thermal evaporation,

Optics EXPRESS

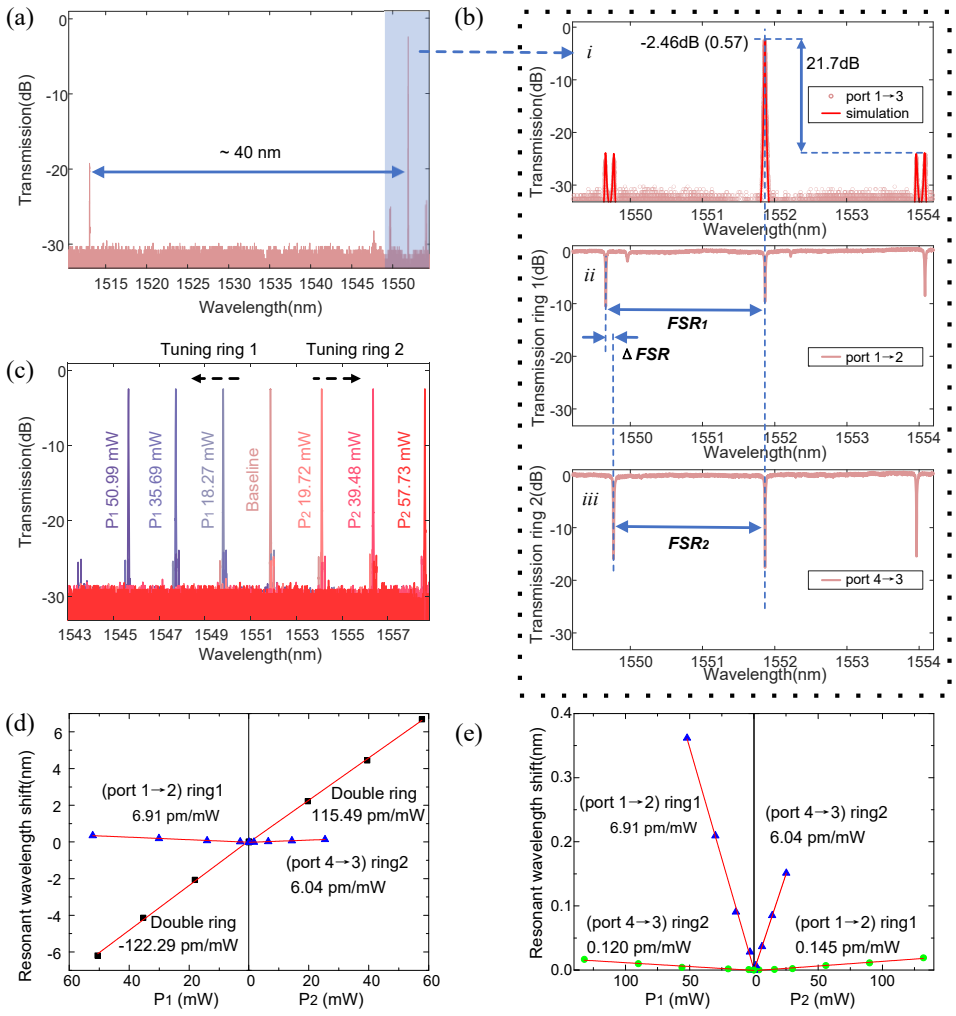

Fig. 2. (a) Measured broadband output spectrum at port 3 when the resonant peaks of the two rings are aligned at the wavelength of around 1550 nm. (b) Top: zoom-in view of the double-ring output spectrum (light red circles) in the blue shaded area in (a), together with simulated results (dark red curve). Middle and bottom: transmission spectra of ring 1 and ring 2 at respective through ports. (c) Measured output transmission spectra at port 3 at various applied thermal power levels showing coarse tuning over a 13 nm range. (d) Measured resonant wavelength shift versus heating power for the full double-ring filter (black squares) and each single ring (blue triangles), respectively. (e) Zoom-in view of the single-ring tuning curves in (d) (blue triangles), in comparison with measured crosstalk between the two rings (green circles). P_1 and P_2 in (d) and (e) are power values applied to ring 1 and ring 2, respectively.

Optics EXPRESS

and lift-off processes. Afterward, a similar lift-off process is conducted to fabricate 1-μm-thick Cu/Au on-chip interconnects and wire-bonding pads. The chips are then cleaved for end-fire optical coupling. Figures 1(b) and (c) depict the microscope images of the fabricated tunable Vernier micro-ring filter with electrodes and wire bonding pads. Finally, we perform wire bonding to realize electrical interconnection between the optical chip and a custom-designed PCB. Figure 1(d) shows the electrically packaged optical filter module under testing, while Fig. 1(e) provides a close-up microscope image of the wire bonding area.

As shown in Fig. 1(a), light with fundamental TE mode input into port 1 can travel through both ring 1 and ring 2 only when the two rings resonate simultaneously, resulting in a high transmission state at the drop port 3. In other scenarios, including the case where only a single ring resonates, the output transmission level at port 3 would be low. In Fig. 2(a) and (b), when the resonance peaks of the two rings are aligned at the wavelength of around 1550 nm, a maximum transmission peak can be observed at the resonant wavelength in the output spectra at port 3. The difference in FSRs of the two rings leads to significant wavelength mismatch at other resonances, and consequently suppressed overall optical transmission. High optical transmission could appear again at an extended Vernier FSR of $FSR_1 \times FSR_2 \,/\, \Delta FSR$ (the peak near 1510 nm in Fig. 2(a)), when the wavelength is $m \times FSR_1$ and $(m+1) \times FSR_2$ away from the original resonance and both rings are on resonance again (m is an integer number). In our device, the extended Vernier FSR is about 40 nm, which is approximately 20 times larger than that of the single ring ($FSR_1 = 2.216$ nm and $FSR_2 = 2.100$ nm), greatly enlarging the single-mode tuning range. All ring-bus waveguide gaps are set to be identical ($g = 600$ nm). Since the rings are fabricated through a single process and are nearly identical, their loaded Q factors (Q_L) are consistent. Specifically, Q_L values of ring 1 and ring 2 are 8.06×10^4 and 7.94×10^4, which correspond to resonance linewidths of 19.3 pm and 19.5 pm (as shown in Fig. 3(a)), respectively. The estimated intrinsic Q factors (Q_i) of the micro-ring resonators are around 6.0×10^5. The large ratio of $Q_i \,/\, Q_L \approx 7.5$ ensures both add-drop rings operate in near critical-coupling states with a high peak optical transmission of 0.57 at the resonant wavelength. Further improvement in optical transmission could be achieved by an improved fabrication process to increase Q_i. Meanwhile, SLSR is determined by the resonant wavelength mismatch at the neighboring mode (ΔFSR) relative to the resonant linewidth ($\lambda \,/\, Q_L$). In our case, the resonance mismatch of 116 pm is about 6 times the resonance linewidth, leading to a large measured SLSR of 21.7 dB (Fig. 2(b)), with good agreement with the simulation results. Overall, there is a good balance between on-resonance optical transmission and SLSR in the designed Vernier micro-ring filter.

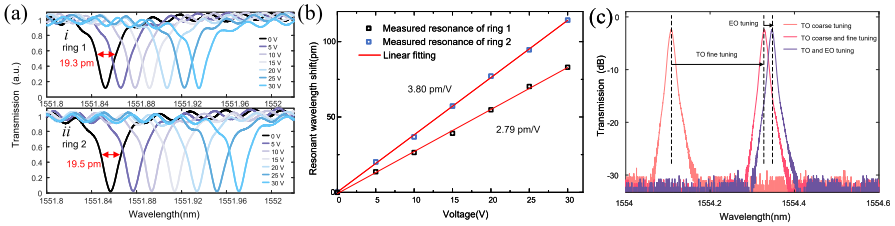

Fig. 3. (a) Measured transmission spectra of ring 1 (i) and ring 2 (ii) at various applied DC voltages, respectively. (b) Resonant wavelength shift of the two rings as functions of applied DC voltages according to (a). (c) Combined TO and EO tuning of the double-ring filter to achieve a target wavelength.

Optics EXPRESS

3. Filter characterization

3.1. TO tuning efficiency

We first evaluate the TO tuning efficiency. A continuous-wave (CW) laser (Santec TSL- 550) is used as the light source. A 3-paddle fiber polarization controller (FPC) is used to ensure the TE mode excitation. Light is butt-coupled into and out of the LNOI chip through lensed fibers, and then the photodetector (PD) translates the optical signals into the electrical domain to display the spectra on the computer. We slowly increase the TO tuning power of ring 1 and first obtain a maximum output at the wavelength of 1551.857 nm (the curve marked "Baseline" in Fig. 2(c)), which means the resonant peaks of the two rings are aligned.

Next, we apply extra thermal power to the TO phase shifter of ring 1 or ring 2 to shift the filter wavelength from the baseline. The applied power values shown in Fig. 2 correspond to additional thermal power applied to the two rings with respect to the baseline. As shown in Fig. 2(c), when tuning ring 2, the resonance peak is red-shifted with a step of FSR_1. This is because every time the resonance peak of ring 2 is redshifted by ΔFSR, the resonance peaks of ring 1 and ring 2 will be realigned with a shift of FSR_1 from the previous resonant peak, effectively increasing the tuning efficiency by 19 times ($FSR_1/\Delta FSR$). Similarly, when tuning ring 1, the resonance peak is blue-shifted with a step of FSR_2. Figure 2(d) shows the resonant wavelength shift of the full double-ring filter (black squares) and each single ring (blue triangles) at different heating powers, all of which feature linear relationships. The tuning efficiency of the double-ring system is 115.5 pm/mW when heating up ring 2 (right half of Fig. 2(d)), which is 19.1 times that of our single ring 2 measured to be 6.04 pm/mW, consistent with the FSR ratios measured above. Similarly, the double-ring tuning efficiency when heating up ring 1 is −122.29 pm/mW (left half of Fig. 2(d)), 17.7 times that of single-ring 1 at 6.91 pm/mW, which is also consistent with the theoretical value of 18 times ($FSR_2/\Delta FSR$). We have also assessed the thermal crosstalk between the two rings by heating one ring and measuring the resonance wavelength shift of the other. As shown in Fig. 2(e), the measured crosstalk tuning efficiency is on the order of 0.1 pm/mW, which is dramatically smaller compared to the TO tuning efficiency of the ring itself.

3.2. EO tuning efficiency

We then demonstrate efficient and linear EO tuning in our double-ring filter. Figures 3(a) and (b) show the measured transmission spectra with different applied direct current (DC) voltages on the EO electrodes of the two rings respectively. The shape of the resonance dips remains largely unchanged, while the resonant wavelength shifts linearly with the applied DC voltage, with measured tuning efficiencies of 2.79 pm/V and 3.80 pm/V for ring 1 and ring 2, respectively. These values are consistent with previously reported EO tuning efficiencies of LNOI microring resonators considering only half of the ring is equipped with EO modulation electrodes in our devices [26]. The difference between the EO tuning efficiencies in the two rings may arise from the EO electrodes and the two rings not being perfectly aligned in fabrication.

3.3. TO and EO tuning

We next demonstrate tuning the Vernier filter with TO and EO effects together, as shown in Fig. 3(c). In general, we can first perform coarse TO tuning by adjusting either ring 2 or ring 1 according to the direction of the wavelength shift, shifting the resonant wavelength by a step of FSR_1 or -FSR_2, respectively. Next, fine-tuning within one FSR can be achieved by simultaneously adjusting both ring 1 and ring 2 until the resonant wavelength is adjusted to the targeted value. Finally, EO tuning of both rings could be performed to locally shift the filter wavelength at high speeds.

In our experiments, we first tune the double rings to the baseline and then apply a heating power of 20 mW to ring 2, redshifting the resonance peak to within one FSR from our target wavelength.

Optics EXPRESS

We subsequently apply a heating power of 29 mW to ring 1 and an additional power of 33 mW to ring 2, positioning the filter near the target wavelength. Finally, we apply DC voltages to the EO electrodes of the two rings to perform EO tuning. When the voltages applied to ring 1 and ring 2 are 7.60 V and 5.69 V, respectively, the resonance wavelength of the double-ring filter shifts by 17.8 pm, which is close to the theoretical shift of 21 pm. The discrepancy may arise from DC drift during the EO testing process. In practical applications, we can use TO electrodes for static tuning of the filter location and use EO electrodes only for high-speed tuning of resonant wavelengths (with zero average bias) to minimize the DC drift issue.

3.4. Tuning speed

We finally measure the switching speeds of our TO and EO phase shifters. We first align the resonances of the two rings and park the input laser at the resonance wavelength, and then apply a periodic electrical square-wave signal generated from an arbitrary waveform generator (AWG) (DG4136 RIGOL) to the TO or EO electrodes of ring 2, causing the optical filter to switch between band-pass and all-stop states. The electrical signals converted from the output optical power by a PD are captured on an oscilloscope (DS6104) in real time. Figure 4(a) illustrates the TO switching characteristics showing rise and fall times of 69 and 8 μs, respectively. The fall time is shorter than the rise time, likely due to faster heating compared to cooling of the heater. The measured TO response time is constrained by the relatively slow thermal build-up and dissipation processes and is also consistent with previous reports in the LNOI platform [34,24].

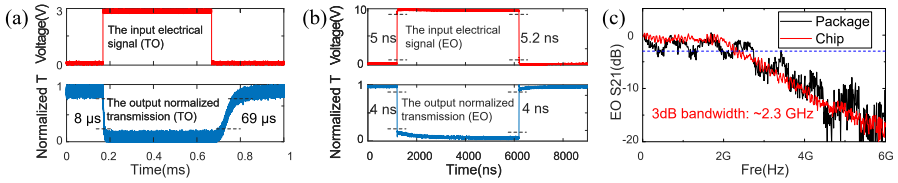

Fig. 4. Measured time-domain responses of the double-ring filter using TO (a) and EO (b) tuning electrodes of ring 2. The red and blue curves correspond to the applied square-wave electrical signals and the normalized output optical signals, respectively. (c) Measured EO S21 responses of the double-ring filter when a small RF signal is applied to ring 2 through a probe (red) and through packaged wire bonds (black).

The μs-level TO response time cannot meet the requirements for high-speed tuning. We next test the rise and fall time of the EO switch using the same setup as discussed above. As Fig. 4(b) shows, the measured response time is ~ 4 ns, three orders of magnitude faster than that of TO tuning. The results are currently limited by the bandwidths of the AWG (160 MHz) used, which is corroborated by the measured rise and fall times of the input electrical signals of ~ 5 ns (red curve of Fig. 4(b)).

To further characterize the actual tuning speed of the EO tunable filter, we measure the small-signal EO S21 response of the device at the chip level and after wire-bonding packaging using a vector network analyzer (VNA) (E5080B), as shown in Fig. 4(c). The measured 3 dB bandwidth (f_{3dB}) is about 2.3 GHz, which corresponds to a response time $\approx 0.35 / f_{3dB} = 0.15$ ns. This is also consistent with the optical bandwidth (2.5 GHz) of the resonator and is limited by the photon lifetime of the resonators. The ripples in the measured EO response of the fully packaged device may be caused by electrical losses and reflections in the wire bonds between the optical chip and PCB.

Optics EXPRESS

4. Conclusion

We have developed an integrated photonic Vernier filter with simultaneous TO and EO tuning capabilities in the LNOI platform. The filter features an overall FSR of about 40 nm, TO tuning efficiencies of 115.49 pm/mW (red shift) and −122.29 pm/mW (blue shift), and a tested EO bandwidth of 2.3 GHz. The combination of TO and EO tuning enables the filter to be coarsely adjusted over a wide range and rapidly tuned locally. Thanks to the high Q_i and engineered Q_L of our micro-rings, we have also achieved a high SLSR of 21.7 dB and a relatively high on-resonance optical transmission of approximately 0.6. Further optimizing the fabrication process to increase the Q_i could lead to even higher on-resonance optical transmission without compromising other metrics. Our devices could become important building blocks on the LNOI platform for applications in next-generation communications, microwave photonic systems, ultrafast tunable lasers, and high-speed photonic neuromorphic computing.

Funding. Research Grants Council, University Grants Committee (CityU 11212721, CityU 11204022, C1002-22Y); Croucher Foundation (9509005).

Disclosures. The authors declare no conflicts of interest.

Data availability. Data underlying the results presented in this paper are not publicly available at this time but may be obtained from the authors upon reasonable request.

References

1. V. V. Vanyukov, G. M. Mikheev, T. N. Mogileva, *et al.*, "Near-IR nonlinear optical filter for optical communication window," Appl. Opt. **54**(11), 3290–3293 (2015).
2. T. Hu, W. Wang, C. Qiu, *et al.*, "Thermally Tunable Filters Based on Third-Order Microring Resonators for WDM Applications," IEEE Photonics Technol. Lett. **24**(6), 524–526 (2012).
3. J. Sharma, Z. Xuan, H. Li, *et al.*, "Silicon Photonic Microring-Based 4 × 112 Gb/s WDM Transmitter With Photocurrent-Based Thermal Control in 28-nm CMOS," IEEE J. Solid-State Circuits **57**(4), 1187–1198 (2022).
4. S. Bélanger-de Villers, D. Hould, and W. Shi, "Ultra-compact DWDM filter tunable across the C-band," in *2019 Optical Fiber Communications Conference and Exhibition (OFC)*, (IEEE, 2019), 1–3.
5. M. Sagues, R. G. Olcina, A. Loayssa, *et al.*, "Multi-tap complex-coefficient incoherent microwave photonic filters based on optical single-sideband modulation and narrow band optical filtering," Opt. Express **16**(1), 295–303 (2008).
6. D. Marpaung, J. Yao, and J. Capmany, "Integrated microwave photonics," Nat. Photonics **13**(2), 80–90 (2019).
7. J. Yao, "Photonics to the rescue: A fresh look at microwave photonic filters," IEEE Microwave Mag. **16**(8), 46–60 (2015).
8. R. W. Ridgway, C. L. Dohrman, and J. A. Conway, "Microwave photonics programs at DARPA," J. Lightwave Technol. **32**(20), 3428–3439 (2014).
9. H. Feng, T. Ge, X. Guo, *et al.*, "Integrated lithium niobate microwave photonic processing engine," Nature **627**(8002), 80–87 (2024).
10. M. Li, L. Chang, L. Wu, *et al.*, "Integrated pockels laser," Nat. Commun. **13**(1), 5344 (2022).
11. V. Snigirev, A. Riedhauser, G. Lihachev, *et al.*, "Ultrafast tunable lasers using lithium niobate integrated photonics," Nature **615**(7952), 411–417 (2023).
12. C. Huang, V. J. Sorger, M. Miscuglio, *et al.*, "Prospects and applications of photonic neural networks," Adv. Phys.: X **7**(1), 1981155 (2022).
13. Q. Xu, D. Fattal, and R. G. Beausoleil, "Silicon microring resonators with 1.5-μm radius," Opt. Express **16**(6), 4309–4315 (2008).
14. S. Dey and S. Mandal, "Modeling and analysis of quadruple optical ring resonator performance as optical filter using Vernier principle," Opt. Commun. **285**(4), 439–446 (2012).
15. Z. Xu, X. Shu, and H. Fu, "Sensitivity enhanced fiber sensor based on a fiber ring microwave photonic filter with the Vernier effect," Opt. Express **25**(18), 21559–21566 (2017).
16. S. J. Choi, Z. Peng, Q. Yang, *et al.*, "Tunable narrow linewidth all-buried heterostructure ring resonator filters using Vernier effects," IEEE Photonics Technol. Lett. **17**(1), 106–108 (2005).
17. L. Jin, M. Li, and J.-J. He, "Highly-sensitive silicon-on-insulator sensor based on two cascaded micro-ring resonators with vernier effect," Opt. Commun. **284**(1), 156–159 (2011).
18. G. Ren, T. Cao, and S. Chen, "Design and analysis of a cascaded microring resonator-based thermo-optical tunable filter with ultralarge free spectrum range and low power consumption," Opt. Eng. **50**(7), 074601 (2011).
19. L. Zhou, X. Zhang, L. Lu, *et al.*, "Tunable Vernier Microring Optical Filters With p-i-p-Type Microheaters," IEEE Photonics J. **5**(4), 6601211 (2013).
20. W. S. Fegadolli, L. Feng, M. M.-U. Rahman, *et al.*, "Experimental demonstration of a reconfigurable silicon thermo-optical device based on spectral tuning of ring resonators for optical signal processing," Opt. Express **22**(3), 3425–3431 (2014).

Optics EXPRESS

21. X. Fang and L. Yang, "Thermal effect analysis of silicon microring optical switch for on-chip interconnect," J. Semicond. **38**(10), 104004 (2017).
22. X. Xue, Y. Xuan, C. Wang, *et al.*, "Thermal tuning of Kerr frequency combs in silicon nitride microring resonators," Opt. Express **24**(1), 687–698 (2016).
23. Y. Ding, S. Tao, X. Wang, *et al.*, "Thermo-optic tunable optical filters with GHz-bandwidth and flat-top passband on thin film lithium niobate platform," Opt. Express **30**(12), 22135–22142 (2022).
24. X. Liu, P. Ying, X. Zhong, *et al.*, "Highly efficient thermo-optic tunable micro-ring resonator based on an LNOI platform," Opt. Lett. **45**(22), 6318–6321 (2020).
25. L. Chen, Q. Xu, M. G. Wood, *et al.*, "Hybrid silicon and lithium niobate electro-optical ring modulator," Optica **1**(2), 112–118 (2014).
26. C. Wang, M. Zhang, B. Stern, *et al.*, "Nanophotonic lithium niobate electro-optic modulators," Opt. Express **26**(2), 1547–1555 (2018).
27. Z. Li, R. N. Wang, G. Lihachev, *et al.*, "High density lithium niobate photonic integrated circuits," Nat. Commun. **14**(1), 4856 (2023).
28. Y. Qi and Y. Li, "Integrated lithium niobate photonics," Nanophotonics **9**(6), 1287–1320 (2020).
29. Y. Hu, M. Yu, B. Buscaino, *et al.*, "High-efficiency and broadband on-chip electro-optic frequency comb generators," Nat. Photonics **16**(10), 679–685 (2022).
30. D. Zhu, L. Shao, M. Yu, *et al.*, "Integrated photonics on thin-film lithium niobate," Adv. Opt. Photonics **13**(2), 242–352 (2021).
31. J. Lin, F. Bo, Y. Cheng, *et al.*, "Advances in on-chip photonic devices based on lithium niobate on insulator," Photonics Res. **8**(12), 1910–1936 (2020).
32. J. Ling, Z. Gao, S. Xue, *et al.*, "Electrically empowered microcomb laser," Nat. Commun. **15**(1), 4192 (2024).
33. M. Zhang, C. Wang, R. Cheng, *et al.*, "Monolithic ultra-high-Q lithium niobate microring resonator," Optica **4**(12), 1536 (2017).
34. M. Wang, J. Li, H. Yao, *et al.*, "Thin-film lithium-niobate modulator with a combined passive bias and thermo-optic bias," Opt. Express **30**(22), 39706–39715 (2022).